Cosmological dynamics of spatially flat Einstein-Gauss-Bonnet models in various dimensions: Low-dimensional Λ -term case

Sergey A. Pavluchenko

Programa de Pós-Graduação em Física, Universidade Federal do Maranhão (UFMA), 65085-580, São Luís, Maranhão, Brazil

In this paper we perform a systematic study of spatially flat [(3+D)+1]-dimensional Einstein-Gauss-Bonnet cosmological models with Λ -term. We consider models that topologically are the product of two flat isotropic subspaces with different scale factors. One of these subspaces is three-dimensional and represents our space and the other is D-dimensional and represents extra dimensions. We consider no Ansatz on the scale factors, which makes our results quite general. With both Einstein-Hilbert and Gauss-Bonnet contributions in play, the cases with D=1 and D=2 have different dynamics due to the different structure of the equations of motion. We analytically study equations of motion in both cases and describe all possible regimes. It is demonstrated that D=1 case does not have physically viable regimes while D=2 has smooth transition from high-energy Kasner to anisotropic exponential regime. This transition occurs for two ranges of α and Λ : $\alpha > 0$, $\Lambda > 0$ with $\alpha\Lambda \leqslant 1/2$ and $\alpha < 0$, $\Lambda > 0$ with $\alpha\Lambda < -3/2$. For the latter case, if $\alpha\Lambda = -3/2$, extra dimensional part has $h \to 0$ and so the size of extra dimensions (in the sense of the scale factor) is reaching constant value. We report substantial differences between D=1 and D=2 cases and between these cases and their vacuum counterparts, describe features of the cases under study and discuss the origin of the differences.

PACS numbers: 04.20.Jb, 04.50.-h, 98.80.-k

I. INTRODUCTION

Einstein's general relativity was formulated more than hundred years ago, but the extradimensional models are even older. Indeed, the first attempt to construct an extra-dimensional model was performed by Nordström [1] in 1914. It was a vector theory that unified Nordström's second gravity theory [2] with Maxwell's electromagnetism. Later in 1915 Einstein introduced General Relativity (GR) [3], but still it took almost four years to prove that Nordström's theory and others were wrong. During the solar eclipse of 1919, the bending of light near the Sun was measured and the deflection angle was in perfect agreement with GR, while Nordström's theory, being scalar gravity, predicted a zeroth deflection angle. But Nordström's idea about extra dimensions survived, and in 1919 Kaluza proposed [4] a similar model but based on GR: in his model five-dimensional Einstein equations could be decomposed into four-dimensional Einstein equations plus Maxwell's electromagnetism. In order to perform such a decomposition, the extra dimensions should be "curled" or compactified into a circle and "cylindrical conditions" should be imposed. Later in 1926, Klein proposed [5, 6] a nice quantum mechanical interpretation of this extra dimension and so the theory called Kaluza-Klein was formally formulated. Back then their theory unified all known interactions at that time. With time, more interactions were known and it became clear that to unify them all, more extra dimensions are needed. Nowadays, one of the promising theories to unify all interactions is M/string theory.

Presence in the Lagrangian of the curvature-squared corrections is one of the distinguishing features of the string theories gravitational counterpart. Indeed, Scherk and Schwarz [7] were the first to discover the potential presence of the R^2 and $R_{\mu\nu}R^{\mu\nu}$ terms in the Lagrangian of the Virasoro-Shapiro model [8, 9]. A curvature squared term of the $R^{\mu\nu\lambda\rho}R_{\mu\nu\lambda\rho}$ type appears [10] in the low-energy limit of the $E_8 \times E_8$ heterotic superstring theory [11] to match the kinetic term for the Yang-Mills field. Later it was demonstrated [12] that the only combination of quadratic terms that leads to a ghost-free nontrivial gravitation interaction is the Gauss-Bonnet (GB) term:

$$L_{GB} = L_2 = R_{\mu\nu\lambda\rho}R^{\mu\nu\lambda\rho} - 4R_{\mu\nu}R^{\mu\nu} + R^2.$$

This term, first found by Lanczos [13, 14] (therefore it is sometimes referred to as the Lanczos term) is an Euler topological invariant in (3+1)-dimensional space-time, but not in (4+1) and higher dimensions. Zumino [15] extended Zwiebach's result on higher-than-squared curvature terms, supporting the idea that the low-energy limit of the unified theory might have a Lagrangian density as a sum of contributions of different powers of curvature. In this regard the Einstein-Gauss-Bonnet (EGB) gravity could be seen as a subcase of more general Lovelock gravity [16], but in the current paper we restrain ourselves with only quadratic corrections and so to the EGB case.

Extra-dimensional theories have one thing in common—one needs to explain where additional dimensions are "hiding", since we do not sense them, at least with the current level of experiments. One of the possible ways to hide extra dimensions, as well as to recover four-dimensional physics, is to build a so-called "spontaneous compactification" solution. Exact static solutions with the metric being a cross product of a (3+1)-dimensional manifold and a constant curvature "inner space" were build for the first time in [17], but with the (3+1)-dimensional manifold being Minkowski (the generalization for a constant curvature Lorentzian manifold was done in [18]). In the context

of cosmology, it is more interesting to consider a spontaneous compactification in the case where the four-dimensional part is given by a Friedmann-Robertson-Walker metric. In this case it is also natural to consider the size of the extra dimensions as time dependent rather than static. Indeed in [19] it was explicitly shown that in order to have a more realistic model one needs to consider the dynamical evolution of the extra-dimensional scale factor. In [18], the equations of motion for compactification with both time-dependent scale factors were written for arbitrary Lovelock order in the special case of a spatially flat metric (the results were further proven in [20]). The results of [18] were reanalyzed for the special case of 10 space-time dimensions in [21]. In [22], the existence of dynamical compactification solutions was studied with the use of Hamiltonian formalism. More recently, efforts to find spontaneous compactifications were made in [23], where the dynamical compactification of the (5+1) Einstein-Gauss-Bonnet model was considered; in [24, 25] with different metric $Ans\"{a}tze$ for scale factors corresponding to (3+1)- and extra-dimensional parts; and in [26–28], where general (e.g., without any Ansatz) scale factors and curved manifolds were considered. Also, apart from cosmology, the recent analysis has focused on properties of black holes in Gauss-Bonnet [29–33] and Lovelock [34–37] gravities, features of gravitational collapse in these theories [38–40], general features of spherical-symmetric solutions [41], and many others.

In the context of finding exact solutions, the most common Ansatz used for the functional form of the scale factor is exponential or power law. Exact solutions with exponential functions for both the (3+1)- and extra-dimensional scale factors were studied for the first time in [42], and an exponentially increasing (3+1)-dimensional scale factor and an exponentially shrinking extra-dimensional scale factor were described. Power-law solutions have been analyzed in [18, 43] and more recently in [20, 44–47] so that there is an almost complete description (see also [48] for useful comments regarding physical branches of the solutions). Solutions with exponential scale factors [49] have been studied in detail, namely, models with both variable [50] and constant [51] volume, developing a general scheme for constructing solutions in EGB; recently [52] this scheme was generalized for general Lovelock gravity of any order and in any dimensions. Also, the stability of the solutions was addressed in [53] (see also [54] for stability of general exponential solutions in EGB gravity), where it was demonstrated that only a handful of the solutions could be called "stable", while the remaining are either unstable or have neutral/marginal stability, and so additional investigation is required.

In order to find all possible regimes of Einstein-Gauss-Bonnet cosmology, it is necessary to go beyond an exponential or power-law *Ansatz* and keep the functional form of the scale factor generic.

We are also particularly interested in models that allow dynamical compactification, so it is natural to consider the metric as the product of a spatially three-dimensional part and an extra-dimensional part. In that case the three-dimensional part represents "our Universe" and we expect for this part to expand while the extra-dimensional part should be suppressed in size with respect to the three-dimensional one. In [26] it was found that there exists a phenomenologically sensible regime in the case when the curvature of the extra dimensions is negative and the Einstein-Gauss-Bonnet theory does not admit a maximally symmetric solution. In this case the three-dimensional Hubble parameter and the extra-dimensional scale factor asymptotically tend to the constant values. In [27] a detailed analysis of the cosmological dynamics in this model with generic couplings was performed. Recently this model was also studied in [28], where it was demonstrated that, with an additional constraint on couplings, Friedmann-type late-time behavior could be restored.

The current paper is a spiritual successor of [55], where we investigated cosmological dynamics of the vacuum Einstein-Gauss-Bonnet model. In both papers the spatial section is a product of two spatially flat manifolds with one of them three-dimensional, which represents our Universe and the other is extra-dimensional. In [55] we considered vacuum model while in the current paper — the model with the cosmological term. In [55] we demonstrated that the vacuum model has two physically viable regimes — first of them is the smooth transition from high-energy GB Kasner to low-energy GR Kasner. This regime appears for $\alpha > 0$ at D = 1, 2 and for $\alpha < 0$ at $D \geqslant 2$ (so that at D = 2 it appears for both signs of α). The other viable regime is smooth transition from high-energy GB Kasner to anisotropic exponential regime with expanding three-dimensional section ("our Universe") and contracting extra dimensions; this regime occurs only for $\alpha > 0$ and at $D \geqslant 2$. Let us note that in [26–28] we considered similar model but with both manifolds to be constant (generally non-zero) curvature. Unlike the paper with vacuum solutions, in this paper we limit ourselves with only lower-dimensional (D = 1 and D = 2) cases; the higher-dimensional cases — D = 3 and the general $D \geqslant 4$ case — will be considered in a separate forthcoming paper.

The structure of the manuscript is as follows: first we write down general equations of motion for Einstein-Gauss-Bonnet gravity, then we rewrite them for our symmetry Ansatz. In the following sections we analyze them for D=1 and D=2 cases, considering the Λ -term case in this paper only. Each case is followed by a small discussion of the results and properties of this particular case; after considering all cases we discuss their properties, generalities, and differences and draw conclusions.

II. EQUATIONS OF MOTION

As mentioned above, we consider the spatially flat anisotropic cosmological model in Einstein-Gauss-Bonnet gravity with Λ -term as a matter source. The equations of motion for such model include both first and second Lovelock contributions and could easily be derived from the general case (see, e.g., [20]). We consider flat anisotropic metric

$$g_{\mu\nu} = \text{diag}\{-1, a_1^2(t), a_2^2(t), \dots, a_N^2(t)\};$$
 (1)

the Lagrangian of this theory has the form

$$\mathcal{L} = R + \alpha \mathcal{L}_2 - 2\Lambda,\tag{2}$$

where R is the Ricci scalar and \mathcal{L}_2 ,

$$\mathcal{L}_2 = R_{\mu\nu\alpha\beta}R^{\mu\nu\alpha\beta} - 4R_{\mu\nu}R^{\mu\nu} + R^2 \tag{3}$$

is the Gauss-Bonnet Lagrangian. Then substituting (1) into the Riemann and Ricci tensors and the scalar in (2) and (3), and varying (2) with respect to the metric, we obtain the equations of motion,

$$2\left[\sum_{\substack{j\neq i}} (\dot{H}_{j} + H_{j}^{2}) + \sum_{\substack{\{k>l\}\\ \neq i}} H_{k}H_{l}\right] + 8\alpha\left[\sum_{\substack{j\neq i}} (\dot{H}_{j} + H_{j}^{2}) \sum_{\substack{\{k>l\}\\ \neq \{i,j\}}} H_{k}H_{l} + 3\sum_{\substack{\{k>l>\\ m>n\}\neq i}} H_{k}H_{l}H_{m}H_{n}\right] - \Lambda = 0$$
(4)

as the *i*th dynamical equation. The first Lovelock term—the Einstein-Hilbert contribution—is in the first set of brackets and the second term—Gauss-Bonnet—is in the second set; α is the coupling constant for the Gauss-Bonnet contribution and we put the corresponding constant for Einstein-Hilbert contribution to unity. Also, since we a consider spatially flat cosmological model, scale factors do not hold much in the physical sense and the equations are rewritten in terms of the Hubble parameters $H_i = \dot{a}_i(t)/a_i(t)$. Apart from the dynamical equations, we write down a constraint equation

$$2\sum_{i>j} H_i H_j + 24\alpha \sum_{i>j>k>l} H_i H_j H_k H_l = \Lambda.$$
(5)

As mentioned in the Introduction, we want to investigate the particular case with the scale factors split into two parts – separately three dimensions (three-dimensional isotropic subspace), which are supposed to represent our world, and the remaining represent the extra dimensions (D-dimensional isotropic subspace). So we put $H_1 = H_2 = H_3 = H$ and $H_4 = \ldots = H_{D+3} = h$ (D designs the number of additional dimensions) and the equations take the following form: the dynamical equation that corresponds to H,

$$2\left[2\dot{H} + 3H^{2} + D\dot{h} + \frac{D(D+1)}{2}h^{2} + 2DHh\right] + 8\alpha \left[2\dot{H}\left(DHh + \frac{D(D-1)}{2}h^{2}\right) + D\dot{h}\left(H^{2} + 2(D-1)Hh + \frac{(D-1)(D-2)}{2}h^{2}\right) + 2DH^{3}h + \frac{D(5D-3)}{2}H^{2}h^{2} + D^{2}(D-1)Hh^{3} + \frac{(D+1)D(D-1)(D-2)}{8}h^{4}\right] - \Lambda = 0,$$
(6)

the dynamical equation that corresponds to h,

$$2\left[3\dot{H} + 6H^{2} + (D-1)\dot{h} + \frac{D(D-1)}{2}h^{2} + 3(D-1)Hh\right] + 8\alpha\left[3\dot{H}\left(H^{2} + 2(D-1)Hh + \frac{(D-1)(D-2)}{2}h^{2}\right) + (D-1)\dot{h}\left(3H^{2} + 3(D-2)Hh + \frac{(D-2)(D-3)}{2}h^{2}\right) + 3H^{4} + \frac{9(D-1)H^{3}h + 3(D-1)(2D-3)H^{2}h^{2} + \frac{3(D-1)^{2}(D-2)}{2}Hh^{3} + \frac{D(D-1)(D-2)(D-3)}{8}h^{4}\right] - \Lambda = 0,$$

$$(7)$$

and the constraint equation,

$$2\left[3H^{2}+3DHh+\frac{D(D-1)}{2}h^{2}\right]+24\alpha\left[DH^{3}h+\frac{3D(D-1)}{2}H^{2}h^{2}+\frac{D(D-1)(D-2)}{2}Hh^{3}+\frac{D(D-1)(D-2)(D-3)}{24}h^{4}\right]=\Lambda. \tag{8}$$

Looking at (6) and (7) one can see that for $D \ge 4$ the equations of motion contain the same terms, while for $D = \{1, 2, 3\}$ the terms are different [say, for D = 3 terms with the (D - 3)

multiplier are absent and so on] and the dynamics should be different also. We are going to study these four cases separately. As we mentioned in the Introduction, in this paper we are going to consider only the Λ -term case; the vacuum case we considered in the previous paper [55] while the general case with a perfect fluid with an arbitrary equation of state we as well as the effect of curvature, are going to be considered in the papers to follow. As we also noted in the Introduction, in this particular paper we consider only $D = \{1, 2\}$ cases – the D = 3 and general $D \geqslant 4$ cases we consider in forthcoming paper.

III.
$$D = 1$$
 CASE

In this case the equations of motion take the form (H-equation, h-equation, and constraint correspondingly)

$$4\dot{H} + 6H^2 + 2\dot{h} + 2h^2 + 4Hh + 8\alpha \left(2(\dot{H} + H^2)Hh + (\dot{h} + h^2)H^2\right) = \Lambda,$$
(9)

$$6\dot{H} + 12H^2 + 24\alpha(\dot{H} + H^2)H^2 = \Lambda, \tag{10}$$

$$6H^2 + 6Hh + 24\alpha H^3 h = \Lambda. {(11)}$$

From (11) we can easily see that

$$h = \frac{\Lambda - 6H^2}{6H(1 + 4\alpha H^2)},\tag{12}$$

and we present them in Fig. 1. In there, panel (a) corresponds to $\alpha > 0$ while both (b) and (c) – to $\alpha < 0$. In all panels black curve corresponds to the typical $\Lambda > 0$ behavior while grey – to $\Lambda < 0$. The difference between (b) and (c) panels is that for black curves in (b) we have $\alpha \Lambda > -3/2$ and in (c) $\alpha \Lambda < -3/2$. The difference in behavior between $\alpha \Lambda > -3/2$ and $\alpha \Lambda < -3/2$ cases manifests itself only for $\alpha < 0$, that is why we have only one curve for $\alpha > 0$. Also, one can see that grey curves in Figs. 12(b) and (c) coincide – they both are for $\alpha < 0$ and $\Lambda < 0$ so for both of them $\alpha \Lambda > -3/2$. Let us also note that for successful compactification one needs H > 0 and $h \leq 0$ so

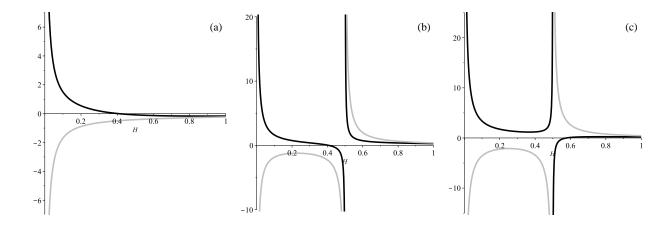


FIG. 1: Behavior of h(H) from Eq. (12) in D=1 case. Panel (a) corresponds to $\alpha>0$ while both (b) and (c) – to $\alpha<0$. In all panels black curve corresponds to the typical $\Lambda>0$ behavior while grey – to $\Lambda<0$. The difference between (b) and (c) panels is that for black curves in (b) we have $\alpha\Lambda>-3/2$ while in (c) $\alpha\Lambda<-3/2$ (see the text for more details).

that from Fig. 1 one can judge about the regions of the initial conditions and parameters where it could be satisfied.

Now with explicit for h(H) we can solve (9)–(10) and substitute (12) into them to get

$$\dot{H} = \frac{\Lambda - 24\alpha H^4 - 12H^2}{6(1 + 4\alpha H^2)},$$

$$\dot{h} = -\frac{576\alpha^2 H^8 - 288\alpha^2 \Lambda H^6 + 144\alpha H^6 - 192\alpha \Lambda H^4 + 12\alpha \Lambda^2 H^2 - 72H^4 - 6\Lambda H^2 + \Lambda^2}{36H^2(1 + 4\alpha H^2)^3}.$$
(13)

Before considering $\dot{H}(H)$ and $\dot{h}(H)$ curves, let us analyze (13), finding their roots and asymptotes. As $\dot{H}(H)$ and $\dot{h}(H)$ have the same denominator, they have the same asymptote located at $(1+4\alpha H^2)=0$, which corresponds to $H^2=-1/(4\alpha)$, which is the same asymptote as from (12), so that $H^2=-1/(4\alpha)$ is nonstandard singularity in this case. As of the roots, they are the following:

$$\dot{H} = 0 \iff H_{\pm}^2 = -\frac{3 \pm \sqrt{6\alpha\Lambda + 9}}{12\alpha},$$

$$\dot{h} = 0 \iff H^2 = -\frac{3 \pm \sqrt{6\alpha\Lambda + 9}}{12\alpha}, \frac{6\alpha\Lambda + 3 \pm \sqrt{36\alpha^2\Lambda^2 + 60\alpha\Lambda + 9}}{24\alpha}.$$
(14)

¹ Nonstandard singularity is the situation when the highest derivative (\dot{H} and/or \dot{h} in our case) diverge while lower derivatives and/or variables are regular. This situation is singular, but due to regularity of lower derivatives and/or variables, it happens some finite time. We discuss this situation more in the Discussions section.

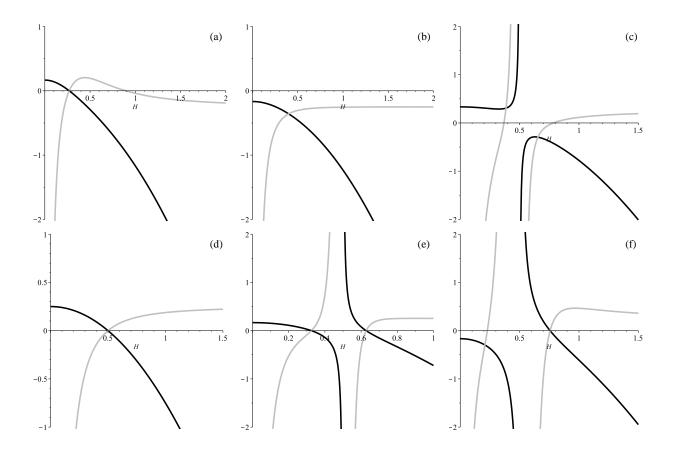


FIG. 2: Behavior of $\dot{H}(H)$ and $\dot{h}(H)$ from Eqs. (13) in D=1 case. In all panels black curve corresponds to $\dot{H}(H)$ and grey curve to $\dot{h}(H)$. Panel (a) corresponds to $\alpha>0$ and $\Lambda>0$ while panel (b) – to $\alpha>0$ and $\Lambda<0$. The remaining panels correspond to $\alpha<0$: $\alpha\Lambda<-3/2$ in (c), $\alpha\Lambda=-3/2$ in (d) and $\alpha\Lambda>-3/2$ in (e). Finally, in (f) panel we presented typical $\alpha<0$, $\Lambda<0$ behavior. (see the text for more details).

Before going further, let us note an interesting fact – roots of $\dot{H}=0$ are the roots of $\dot{h}=0$ as well, so they determine exponential solutions allowed in this case. If we substitute corresponding H from (14) into (12), we can note that both of them have h=H. So that in D=1 case we have two exponential solutions and both of them are isotropic – which is very different from the vacuum case.

Having this in mind, we can now plot $\dot{H}(H)$ and $\dot{h}(H)$ curves in Fig. 2 and analyze them. In all panels black curves correspond to $\dot{H}(H)$ and grey curves to $\dot{h}(H)$. Panel (a) corresponds to $\alpha > 0$ and $\Lambda > 0$ while panel (b) – to $\alpha > 0$ and $\Lambda < 0$. The remaining panels correspond to $\alpha < 0$: $\alpha \Lambda < -3/2$ in (c), $\alpha \Lambda = -3/2$ in (d) and $\alpha \Lambda > -3/2$ in (e). Finally, in (f) panel we presented typical $\alpha < 0$, $\Lambda < 0$ behavior.

One important remark on the notations – hereafter we are using notations we used in [55]. So

we denote exponential solutions as E with subindices which indicate specifics of the solution, e.g., E_{iso} is isotropic exponential solution and so on. Power-law solutions generally denoted as K as a reference to Kasner regime with K_1 being low-energy or GR Kasner regime, governed by $\sum p_i = 1$ and $\sum p_i^2 = 1$. High-energy or Gauss-Bonnet Kasner regime is denoted as K_3 as it has $\sum p_i = 3$. Finally we denote nonstandard singularity of any nature as nS – in [55] we detected several different types of nonstandard singularities, and expect in current paper to have variety of them as well, but without discrimination we denote all of them as nS.

Now let us have closer look on individual panels. In (a) panel we presented behavior for $\alpha > 0$ and $\Lambda > 0$ case. One can see that we have stable point which is isotropic exponential solution (since $\dot{H} = 0$ and $\dot{h} = 0$) with two different past asymptotes. A bit further, when analyzing the behavior in Kasner exponents, we demonstrate that one of them (at $H \to \infty$) is Gauss-Bonnet Kasner K_3 and the other is similar to usual (general relativity) Kasner regimes K_1 . Since this solution is similar to K_1 but not exactly low-energy Kasner, we denote it as \tilde{K}_1 and discuss it later in the Discussion section. The next (b) panel corresponds to $\alpha > 0$ and $\Lambda < 0$ case. We can see that in this case $\dot{H} < 0$ always so it is singular transition from GB to GR Kasner-like regimes (as we demonstrate further with Kasner exponents). All remaining panels correspond to $\alpha < 0$ case and first of them to consider is (c) panel with $\alpha \Lambda < -3/2$. There we can see two singular regimes with nonstandard singularity at $H^2 = -1/(4\alpha)$ as future attractor: first of them, at lower H, has low-energy Kasner-like regime as past attractor while the second, with higher H, has high-energy Kasner; a bit further we demonstrate it with Kasner exponents. Next, exact $\alpha\Lambda = -3/2$ case in (d) panel, and it is quite similar to the case in Fig. 2 (a) – the same isotropic exponential solution with two different Kasner regimes as past attractors. The next case is more interesting and it is presented in (e) panel – the case with $\alpha\Lambda > -3/2$. There we can see two distinct isotropic exponential solutions – the situation we never saw in the vacuum case [55]. So the the lower Hpart we have two regimes – \tilde{K}_1 to the first isotropic solution $E_{iso}^{(1)}$ and nonstandard singularity to $E_{iso}^{(1)}$; the higher H part is quite similar but with K_3 instead of \tilde{K}_1 . Finally, in (f) panel we have $\alpha < 0, \, \Lambda < 0$ case. Its low-H part has nS to \tilde{K}_1 transition while high-H has two – nS to E_{iso} and K_3 to E_{iso} .

This finalize our analysis of $\dot{H}(H)$ and $\dot{h}(H)$ curves, but to clarify Kasner regimes we perform analysis of the Kasner exponents as well. They are defined from the power-law ansatz as $a(t) \propto t^p$ with p being Kasner exponent and could be reexpressed as $p = -H^2/\dot{H}$. Now with use of (13) we can express p_H (Kasner exponent which corresponds to H) and p_h (the same but for h) explicitly:

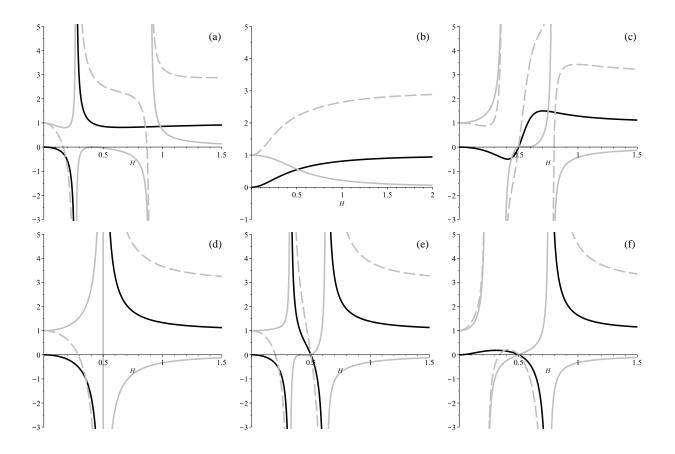


FIG. 3: Behavior of Kasner exponents from Eq. (15) in D=1 case. On all panels black curve corresponds to p_H , solid grey curve – to p_h and dashed grey – to the expansion rate $\sum p=3p_H+p_h$. Panel (a) corresponds to $\alpha>0$ and $\Lambda>0$ while panel (b) – to $\alpha>0$ and $\Lambda<0$. The remaining panels correspond to $\alpha<0$: $\alpha\Lambda<-3/2$ in (c), $\alpha\Lambda=-3/2$ in (d) and $\alpha\Lambda>-3/2$ in (e). Finally, in (f) panel we presented typical $\alpha<0$, $\Lambda<0$ behavior. (see the text for more details).

$$p_H = -\frac{H^2}{\dot{H}} = \frac{6H^2(1 + 4\alpha H^2)}{24\alpha H^4 + 12H^2 - \Lambda},$$

$$p_h = -\frac{h^2}{\dot{h}} = \frac{(1 + 4\alpha H^2)(\Lambda - 6H^2)^2}{576\alpha^2 H^8 - 288\alpha^2 \Lambda H^6 + 144\alpha H^6 - 192\alpha \Lambda H^4 + 12\alpha \Lambda^2 H^2 - 72H^4 - 6\Lambda H^2 + \Lambda^2}.$$
(15)

We plot the resulting curves in Fig. 3. There on all panels black curve corresponds to p_H , solid grey curve – to p_h and dashed grey – to the expansion rate $\sum p = 3p_H + p_h$. The panels layout is the same as in Fig. 2 – panel (a) corresponds to $\alpha > 0$, $\Lambda > 0$; panel (b) – to $\alpha > 0$, $\Lambda < 0$; panel (c) – to $\alpha < 0$, $\Lambda > 0$ and $\alpha \Lambda < -3/2$; panel (d) – to $\alpha < 0$, $\Lambda > 0$ and $\alpha \Lambda = -3/2$; panel (e) – to $\alpha < 0$, $\Lambda > 0$ and $\alpha \Lambda > -3/2$ and panel (f) – to $\alpha < 0$, $\Lambda < 0$.

Before comparing the dynamics in $\{\dot{H},\dot{h}\}$ coordinates from Fig. 2 with the dynamics in $\{p_H,p_h\}$ coordinates from Fig. 3, let us make several notes. First of all, from the definition of the Kasner exponent $p = -H^2/\dot{H}$ any point where $\dot{H} = 0$ becomes singular for p (except for H = 0 sometimes), which do not corresponds to any physical singularities in $\{\dot{H},\dot{h}\}$ description. So that the description in $\{p_H,p_h\}$ coordinates could create "fake" singularities. Actually, H = 0 corresponds to the exponential solution, so divergences in $\{p_H,p_h\}$ coordinates correspond to them as well. Secondly, again from the Kasner exponent definition, there could be a situation when at physical singularity both H and \dot{H} diverge in a way for p to remains regular – so that the description in $\{p_H,p_h\}$ coordinates could not only create "fake" singularities, but also "hide" physical ones, and in the vacuum case [55] we described several situations like that. All these makes $\{p_H,p_h\}$ description flawed, but we still use it with appropriate care to find power-law asymptotes.

The limiting values for p_H and p_h could be both seen from the Fig. 3 and by taking appropriate limit of (15); one can demonstrate that for K_1 we have $p_H = 0, p_h = 1, \sum p = 1$ while for K_3 we have $p_H = 1, p_h = 0, \sum p = 3$. One can easily confirm that with Fig. 3.

As we just mentioned, exponential solutions in $\{p_H, p_h\}$ coordinates are singularities and so correspond to vertical asymptotes. Apart from them we also have zeros of p_i and they correspond to nonstandard singularities. Indeed, as we define nonstandard singularity as the situation when \dot{H} diverges while H is regular and (generally) nonzero, from the definition of the Kasner exponent $p = -H^2/\dot{H}$ we can clearly see that for $\dot{H} = \pm \infty$ and $H \neq 0$ we have p = 0.

So comparing Fig. 2(a) with Fig. 3(a) we can clearly see both Kasner asymptotes and detect correct values for the expansion rate for both of them ($\sum p = 1$ for K_1 and $\sum p = 3$ for K_3). Also we can see exponential solution where Kasner exponents diverge (see, e.g., [48] for the relations between power-law and exponential solutions) as well as "fake" singularity for p_h where just $\dot{h} = 0$. Comparison of Fig. 2(b) and Fig. 3(b) clearly demonstrate $K_3 \to \tilde{K}_1$ transition. From the comparison of (c) panels we again can see proper power-law behavior at $H \to 0$ and $H \to \infty$ as well as nonstandard singularity where $p_H = p_h = 0$. The (d) panels are similar to (a) – same \tilde{K}_1 and K_3 separated by the exponential solution. The panel (e) of Fig. 3 is a bit more complicated – as its counterpart from Fig. 2 – we detect \tilde{K}_1 and K_3 , two exponential solutions and nonstandard singularity "between" them – all from both Fig. 2(e) and Fig. 3(e). Finally, in (f) panel, apart from \tilde{K}_1 and K_3 we can see exponential solution and nonstandard singularity. All this comparison demonstrates that the descriptions in $\{\dot{H}, \dot{h}\}$ and $\{p_H, p_h\}$ coordinates correspond to each other and adequately describe the dynamics of the system.

TABLE I: Summary of D=1 Λ -term regimes.

α	Λ	Additional conditions		Regimes
$\alpha > 0$	$\Lambda > 0$	$H < H_{-}$ from (14)		$\tilde{K}_1 \to E_{iso}$
		$H > H_{-} \text{ from (14)}$		$K_3 \to E_{iso}$
	$\Lambda < 0$	no		$K_3 \to \tilde{K}_1^S$
	$\Lambda > 0$	$\alpha \Lambda < -3/2$ $H < \frac{1}{2\sqrt{-\alpha}}$ $H > \frac{1}{2\sqrt{-\alpha}}$	$H < \frac{1}{2\sqrt{-\alpha}}$	$\tilde{K}_1 \to nS$
			$H > \frac{1}{2\sqrt{-\alpha}}$	$K_3 \to nS$
		$\alpha \Lambda = -3/2$	$H < \frac{1}{2\sqrt{-\alpha}}$	$\tilde{K}_1 \to E_{iso}$
			$H > \frac{1}{2\sqrt{-\alpha}}$	$K_3 \to E_{iso}$
		$\alpha\Lambda > -3/2$	$H < H_{-} \text{ from (14)}$	$\tilde{K}_1 \to E_{iso}^{(1)}$
$\alpha > 0$			$\frac{1}{2\sqrt{-\alpha}} > H > H_{-} \text{ from (14)}$	$nS \to E_{iso}^{(1)}$
			$\frac{1}{2\sqrt{-\alpha}} > H > H_{-} \text{ from (14)}$ $H_{+} > H > \frac{1}{2\sqrt{-\alpha}} \text{ from (14)}$	$nS \to E_{iso}^{(2)}$
			$H > H_+$ from (14)	$K_3 \to E_{iso}^{(2)}$
	$\Lambda < 0$	$H < \frac{1}{2\sqrt{-\alpha}}$		$nS \to \tilde{K}_1^S$
		$H_{+} > H > \frac{1}{2\sqrt{-\alpha}} \text{ from (14)}$		$nS \to E_{iso}$
		I.	$H > H_+ \text{ from (14)}$	$K_3 \to E_{iso}$

Now let us summarize all regimes found in Table I. We can see a variety of different regimes — much more than we have in D=1 vacuum regime [55]. Almost all of the regimes are singular with the only nonsingular regime $K_3 \to E_{iso}$. But we cannot call it viable — indeed, isotropisation here means equality of all four space dimensions which clearly violate our observations. So we report that, despite of a variety of regimes presented in Table I, none of them is viable — the situation we never had in vacuum case. Also we need to stress readers' attention on power-law solutions once again — as we noted, \tilde{K}_1 is a regime similar to GR Kasner regime K_1 but singular — indeed, from Fig. 1 one can see that upon approaching H=0 we have divergence in \dot{h} — so that H=0 is singular point while "true" Kasner regime (in Bianchi-I, where it was originally defined) is nonsingular. But as H=0 is approached in "nearly Kasner" manner, we denote this regime as \tilde{K}_1 . When this regime is the past attractor, we denote it as \tilde{K}_1^S to stress that it is singular, unlike "usual" K_1 Kasner we saw in the vacuum case [55]. All these issues are discussed in Discussion section.

IV.
$$D = 2$$
 CASE

In this case the equations of motion take the form (H-equation, h-equation, and constraint correspondingly)

$$4\dot{H} + 6H^2 + 4\dot{h} + 6h^2 + 8Hh + 8\alpha \left(2(\dot{H} + H^2)(2Hh + h^2) + 2(\dot{h} + h^2)(H^2 + 2Hh) + 3H^2h^2 \right) = \Lambda,$$
(16)

$$6\dot{H} + 12H^2 + 2\dot{h} + 2h^2 + 6Hh + 8\alpha \left(3(\dot{H} + H^2)(H^2 + 2Hh) + 3(\dot{h} + h^2)H^2 + 3H^3h\right) = \Lambda,$$
(17)

$$6H^2 + 12Hh + 2h^2 + 24\alpha(2H^3h + 3H^2h^2) = \Lambda. \tag{18}$$

If we solve (18) with respect to h we get

$$h_{\pm} = -\frac{24\alpha H^3 + 6H \pm \sqrt{576\alpha^2 H^6 - 144\alpha H^4 + 24H^2(1 + 3\alpha\Lambda) + 2\Lambda}}{2(1 + 36\alpha H^2)}.$$
 (19)

Let us first have a closer look on the radicand in (19). It is bicubic equation with discriminant

$$\Delta = -3981312(6\xi + 1)^2(6\xi + 5),\tag{20}$$

where $\xi = \alpha \Lambda$. As we know, if the discriminant of the cubic equation is positive – it has three real roots, if negative – only one real root. So that for $\xi > -5/6$ we have one and for $\xi < -5/6$ we have three roots. But since the equation is bicubic, not only the number but the sign of the roots is important, so we plot in Fig. 4(a, b) behavior of the radicand from (19) for H > 0. The cases presented on panel (a) are for $\alpha > 0$: $\Lambda > 0$ as black line and $\Lambda < 0$ as grey line. One can see that the former of them has H > 0 as a domain of definition (which defined from the positivity of the radicand) while the latter has only $H > H_1 > 0$. On the next, (b) panel, we presented radicand behavior for $\alpha < 0$ case: $\Lambda > 0$, $\alpha \Lambda < -5/6$ as black line, $\Lambda > 0$, $\alpha \Lambda > -5/6$ as solid grey line and $\Lambda < 0$ as dashed grey line. One can see that, similar to D = 1 case, only $\alpha < 0$ cases are affected by $\alpha \Lambda = -5/6$ separation. So we can see that the $\Lambda > 0$, $\alpha \Lambda < -5/6$ case has twofold discontinuous domain of definition – $0 < H < H_1$ and $H > H_2$ with both H_1 and H_2 defined from the roots of

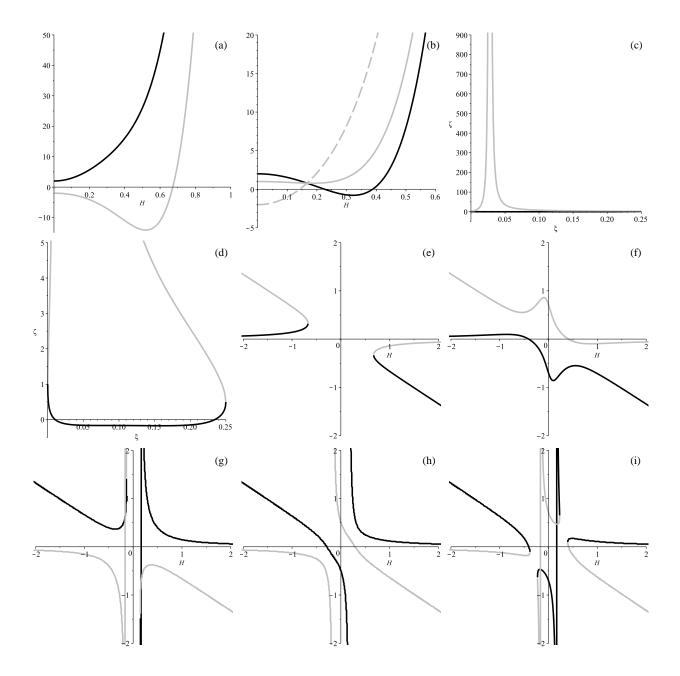


FIG. 4: Behavior of the radicand from (19) in (a) and (b) panels, reduced denominator (26) in (c) and (d) panels and h(H) curves from (19) for different cases in (e)–(i) panels for D=2 case. (see the text for more details).

the radicand. The $\Lambda > 0$, $\alpha \Lambda > -5/6$ case has entire H > 0 as a domain of definition and $\Lambda < 0$ case has $H > H_1 > 0$, similar to $\alpha > 0$, $\Lambda < 0$ case.

With that at hand we can plot h(H) curves from (19). They are presented in (e)–(i) panels of Fig. 4. On all panels black curve corresponds to h_+ while grey – to h_- . So on (e) panel we

presented $\alpha > 0$, $\Lambda < 0$ case – and according to (a) panel, its domain of definition is $H > H_1 > 0$. One can also see that branches "turn" into each other, making impossible entire evolution – we demonstrate it more explicitly later. On (f) panel we presented $\alpha > 0$, $\Lambda > 0$ case and it has entire H > 0 as its domain of definition; branches are also separated from each other. Remaining three panels correspond to $\alpha < 0$: $\Lambda < 0$ on (g), $\Lambda > 0$, $\alpha \Lambda > -5/6$ on (h) and $\Lambda > 0$, $\alpha \Lambda < -5/6$ on (i). One can clearly see that their domains of definition are in accordance with radicand classification. Let us make a note similar to the D = 1 case – for successful compactification one needs H > 0 and $h \leq 0$ so that from Fig. 4 one can judge about the regions of the initial conditions and parameters where it could be satisfied.

Now with h(H) behavior described, we can turn our attention to $\dot{H}(H)$ and $\dot{h}(H)$ behavior. We solve (16)–(17) with respect to \dot{H} and \dot{h} and substitute (19) to get the following expressions:

$$\dot{H}_{\pm} = -\frac{H^2 P_{\pm}^H}{4Q_{\pm}},
\dot{h}_{\pm} = \frac{3H^2 P_{\pm}^h}{4(1 + 36\alpha H^2)^2 Q_{\pm}}$$
(21)

with

$$\begin{split} P_{\pm}^{H} &= 96768\xi^{5} + (\mp 1152\mathcal{D} - 19584)\xi^{4} + (\mp 1248\mathcal{D} + 12096\zeta + 2592)\xi^{3} + \\ &+ (\pm 144\zeta\mathcal{D} \mp 64\mathcal{D} + 912\zeta + 264)\xi^{2} + (\pm 4\zeta\mathcal{D} \mp 4\mathcal{D} - 20\zeta - 12)\xi - \zeta; \\ P_{\pm}^{h} &= 9953280\xi^{7} + (-9787392 \pm 414720\mathcal{D})\xi^{6} + (580608 + 2737152\zeta \mp 76032\mathcal{D})\xi^{5} + \\ &+ (\mp 51840\zeta\mathcal{D} \mp 12096\mathcal{D} + 449280\zeta + 158976)\xi^{4} + (\mp 8352\zeta\mathcal{D} - 62208\zeta^{2} \mp 1296\mathcal{D} + \\ &+ 3456\zeta + 672)\xi^{3} + (\pm 168\zeta\mathcal{D} - 3456\zeta^{2} \pm 160\mathcal{D} + 3552\zeta + 1064)\xi^{2} + \\ &+ (\pm 10\zeta\mathcal{D} - 48\zeta^{2} \mp 6\mathcal{D} + 68\zeta - 28)\xi - \zeta; \\ Q_{\pm} &= 31104\xi^{4} - 2880\xi^{3} + (1296\zeta + 216 \mp 192\mathcal{D})\xi^{2} + (\mp 16\mathcal{D} - 12)\xi - \zeta + 1; \end{split}$$

where $\xi = \alpha H^2$, $\zeta = \alpha \Lambda$ and $\mathcal{D} = \sqrt{576\xi^2 + 72\zeta - 144\xi + 24 + 2\zeta/\xi}$. Before moving forward it is useful to analyze (22) and find their roots to locate zeros and asymptotes of \dot{H} and \dot{h} . One can demonstrate that P_+^H could be rewritten in a form

$$P_+^H \Leftrightarrow (120\xi^2 + 20\xi - \zeta)(192\xi^3 - 112\xi^2 + 4\xi(1+8\zeta) - 1)(288\xi^3 - 72\xi^2 + 12\xi(1+3\zeta) + \zeta),$$
 (23) so it have up to six real roots in five regions divided by four isolated points: $\xi = \{-5/6, -1/6, 15/32, 1/2\}.$ Its counterpart P_-^H has the same roots plus an additional root at $\xi = -1/36$. Similarly, one can demonstrate that P_+^h could be rewritten in a form

$$P_{+}^{h} \Leftrightarrow (120\xi^{2} - 20\xi - \zeta)(120\xi^{2} + 20\xi - \zeta)(144\xi^{2} - 36\xi(1 + 2\zeta) + 1) \times \times (192\xi^{3} - 112\xi^{2} + 4\xi(1 + 8\zeta) - 1), \tag{24}$$

and it have up to nine real roots in five regions divided by the same four isolated points: $\xi = \{-5/6, -1/6, 15/32, 1/2\}$. Similarly to P_-^H , P_-^h has the same as P_+^h roots plus an additional root at $\xi = -1/36$.

As joint roots $\dot{h} = 0$ and $\dot{H} = 0$ determine the locations of exponential solutions, it is important to find them. Comparison of (23) with (24) clearly pinpoints the equation that governs the locations of the exponential solutions:

$$(120\xi^{2} + 20\xi - \zeta) \times (192\xi^{3} - 112\xi^{2} + 4\xi(1 + 8\zeta) - 1) = 0$$

$$\xi_{\pm} = -\frac{1}{12} \pm \frac{\sqrt{30\zeta + 25}}{60},$$

$$\xi_{1} = -\frac{1}{36} \left(-756\zeta + 370 + 18\sqrt{1152\zeta^{3} - 156\zeta^{2} - 660\zeta + 225} \right)^{1/3} - \frac{18\zeta - 10}{9\left(-756\zeta + 370 + 18\sqrt{1152\zeta^{3} - 156\zeta^{2} - 660\zeta + 225} \right)^{1/3}} + \frac{7}{36}, \ \xi_{2,3},$$

$$(25)$$

where ξ_{\pm} are roots of quadratic equation, ξ_1 is the first (always real) root of the cubic equation while $\xi_2 > \xi_3$ are two remaining roots of cubic equation. Analyzing them separately for positive and negative α and Λ , we can conclude: for $\alpha > 0$, $\Lambda > 0$ we have ξ_+ governs location of the exponential solution for h_- while roots of cubic equation govern locations of exponential solutions for h_+ : there is one solution for $\zeta < 15/32$ and $\zeta > 1/2$, two solutions for $\zeta = 15/32$, 1/2 and three solutions for $15/32 < \zeta < 1/2$. For $\alpha > 0$ and $\Lambda < 0$ we have one exponential solution for h_+ which is governed by ξ_- . For $\alpha < 0$, $\Lambda > 0$ the situation is following: for $\zeta > -5/6$ we have two exponential solutions governed by ξ_\pm ; for $\zeta = -5/6$ there remains only one solution (at that point these two roots coincide) and for $\zeta < -5/6$ there are two exponential solutions governed by ξ_2 , $\zeta = 1/2$ (for $\zeta \to -5/6 + 0$ lim $\zeta = 1/2$) so the roots smoothly transit into each other). One of these roots corresponds to $\zeta = 1/2$ and the other $\zeta = 1/2$ to $\zeta = 1/2$ and $\zeta = 1/2$ there are two exponential solutions governed by $\zeta = 1/2$ there are two exponential solutions governed by $\zeta = 1/2$ there are two exponential solutions governed by $\zeta = 1/2$ and the other $\zeta = 1/2$ there are two exponential solutions governed by $\zeta = 1/2$ there are two exponential solutions governed by $\zeta = 1/2$ the first ζ

Finally, let us consider the denominator Q_{\pm} . It could be reduced to sixth order algebraic

equation with respect to ξ but unlike numerators cannot be solved explicitly. But we could solve Q_+ with respect to ζ :

$$\zeta_{\pm} = -\frac{31104\xi^4 - 4608\xi^3 - 600\xi^2 - 172\xi - 1 \pm 16(12\xi + 1)^2\sqrt{-2\xi(4\xi - 1)}}{1296\xi^2 - 72\xi + 1}.$$
 (26)

We plot both branches $-\zeta_+$ as black and ζ_- as grey - in Fig. 4(c, d). There on (c) panel we presented large-scale structure of ζ_- and in (d) - fine structure of ζ_+ . One can see that ζ_- never crosses zero while ζ_+ do. Also, similar to numerators, Q_- has additional root at $\xi = -1/36$. Further analyzing Q_\pm and (26) leads us to the following conclusions: for $\alpha > 0$ and $\Lambda < 0$, Q_+ does not have roots for $\zeta < \zeta_0 \approx -0.17359961^2$, have one for $\zeta = \zeta_0$ and have two for $\zeta > \zeta_0$; Q_- has no roots for $\zeta < 1$ and $\alpha > 0$, has one at H = 0 at $\zeta = 1$ and one at H > 0 at $\zeta > 1$. At $\alpha < 0$ neither of Q_\pm have zeros. For future use we denote $\xi_4 > \xi_5$ as Eq. (26) roots: to each particular ζ they could be found numerically.

With all this preliminary considerations done, it is time to present $\dot{H}(H)$ and $\dot{h}(H)$ curves for all possible distinct areas of parameters. We presented these curves in Figs. 5–7. In all these figures black curves correspond to $\dot{H}(H)$ while grey – to $\dot{h}(H)$. Let us have a closer look on all panels in all figures.

In Fig. 5(a, b) we presented the situation for $\alpha > 0$ and $\zeta < \zeta_0$ mentioned above $(\zeta_0 \approx -0.17359961) - h_+$ in (a) panel and h_- in (b). We can see that the domain of definition does not reach H=0, all according to h(H) graphs investigation. We can see anisotropic exponential solution in (a) panel – it could be verified by taking appropriate root from (23) and (24) and substituting it into h_+ . Apart from it, we can see K_3 regime at high H and nonstandard singularity. On (b) panel we can see the singular transition from K_3 to another nS. On panel (c) we presented behavior for h_+ for $\alpha > 0$ and $0 > \zeta > \zeta_0$, $\zeta \neq 1/6$. We can see more complicated behavior there – some singular behavior between two different singularities, again singular behavior between two different nonstandard singularities followed by nS to anisotropic exponential solution transition and K_3 to this exponential solution. Another branch h_- has the same behavior as in $\zeta < \zeta_0$ case so we do not present it again. On the following (d) and (e) panels we present $\zeta = -1/6$ case – h_+ branch on (d) and h_- branch on (e). On the former of them we can see singular transition followed by nS to anisotropic exponential regime and K_3 to anisotropic exponential solution transitions. On (e) panel we see transition from K_3 to nS. This finalize our study of $\alpha > 0$ $\Lambda < 0$ regimes

 $^{^{2}}$ This value was obtained numerically – as the original equation is sixth order it is impossible to solve it in radicals.

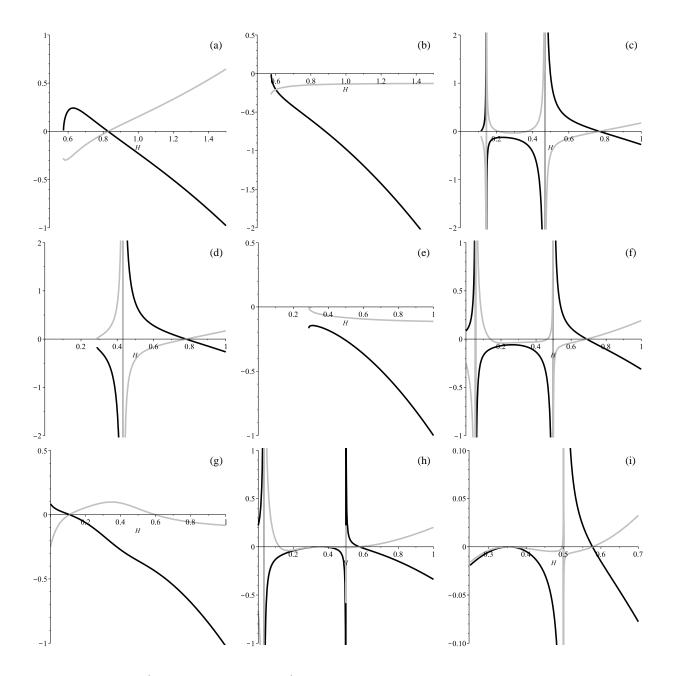


FIG. 5: Behavior of $\dot{H}(H)$ (black curve) and $\dot{h}(H)$ (grey curve) in D=2 case for $\alpha>0$ and: $\zeta<\zeta_0$ on (a) and (b) panels; $0>\zeta>\zeta_0, \ \zeta\neq-1/6$ on (c) panel; $\zeta=-1/6$ on (d) and (e) panels; $0<\zeta<15/32$ on (f) and (g) panels; $\zeta=15/32$ on (h) and (i) panels (see the text for more details).

and we turn to $\alpha > 0$ $\Lambda > 0$ ones. First of them presented in Fig. 5(f, g) and it is $0 < \zeta < 15/32$ case: on (f) panel we have h_+ and on (g) h_- branches. We see that turning to $\Lambda > 0$ changed the domain of definition and now it is entire H > 0. So the regimes on (f) panels are: some power-law to nonstandard singularity, nS to nS and anisotropic exponential solution as future attractor for

nS and K_3 . But what we see as some power-law regime at low H in reality is something else – indeed, from Fig. 4(e)-(i) one can see that in this case (and some other further cases) H=0 is regular and nonzero point for h. So that H=0 is not an endpoint and the evolution must be prolonged to H < 0 domain. As (21)–(24) are symmetric with respect to H = 0 (they contain only even powers of H), one can restore entire H(H) and h(H) graphs by mirroring H>0 part with respect to H=0. Then we can see that the past attractor in this case is nonstandard singularity $nS^{(-)}$, dual to the closest to H=0 nonstandard singularity. On (g) panel we have the behavior for h_{-} which is typical for all $1 > \zeta > 0$ – isotropic exponential solution as future attractor and K_3 for large H. For small H, with the same reasoning as in (f) case, we retrieve $E_{iso}^{(-)}$ – isotropic shrinking, dual to exponential expansion E_{iso} from future attractor. So that in a sense this regime is a bounce from isotropic exponential contraction to isotropic exponential expansion. Finally on (h) and (i) panels of Fig. 5 we presented behavior for h_+ for $\zeta = 15/32$ (as we mentioned, $h_$ branch has behavior similar to presented on (g) panel). From (h) panel one can see that it resemble (f) panel, but the top between nonstandard singularities now "touches" H = 0 line, as seen on (i) panel, creating second anisotropic solution between two nonstandard singularities. So now the solutions include $nS^{(-)}$ to nS at lowest H, then exponential solution to nS transition, nS to this exponential solution transition (this exponential solution at $H = H_0$ has directional stability – it is stable for $H \to H_0 + 0$ but unstable for $H \to H_0 - 0$, nS to another anisotropic exponential solution and K_3 to this solution. So in this case we have two different anisotropic solutions – one of them has directional stability while another is stable.

The description of all regimes continues in Fig. 6. There on (a) and (b) panels we presented the behavior for $1/2 > \zeta > 15/32$. Comparing them with Fig. 5(f, g) one can see that the "touch" from $\zeta = 15/32$ case now moved upper creating two exponential solutions, as seen on (b) panel. So in this case the regimes are: $nS^{(-)}$ to nS at lowest H, the first exponential solution to nS, the first exponential solution to the second exponential solution, nS to the second exponential solution, nS to the third exponential solution and K_3 to it. We see that in that case we have three different anisotropic exponential solutions, and all of them have H > 0 with h < 0. This is so far the most exceptional situation which we never saw in the vacuum case [55]. Of these three exponential solutions, the first one is unstable while the second and third are stable. Our description continues to the $\zeta = 1/2$ case presented on panels (c) and (d). We can see that the second nonstandard singularity is "gone" (or, rather, "moved" to $H = \infty$) so we have $nS^{(-)}$ to nS at lowest H, first exponential solution to nS, first exponential solution to the second exponential solution and K_3 to

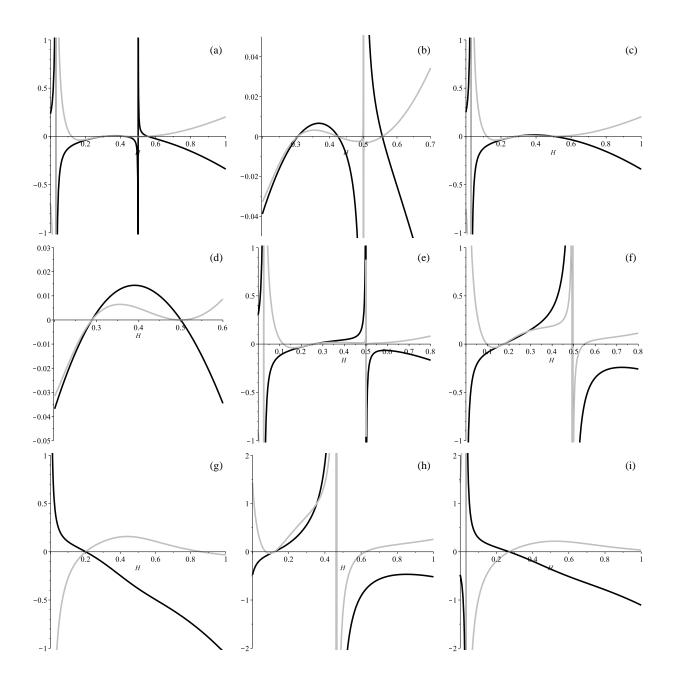


FIG. 6: Continuation of Fig. 5 for $\alpha > 0$ and: $1/2 > \zeta > 15/32$ on (a) and (b) panels; $\zeta = 1/2$ on (c) and (d) panels; $1 > \zeta > 1/2$ on (e) panel; $\zeta = 1$ on (f) and (g) panels; $\zeta > 1$ on (h) and (i) panels (see the text for more details).

the second exponential solution. Next is the $1 > \zeta > 1/2$ case which is presented in Fig. 6(e). We see that the second nonstandard singularity is back and the regimes include $nS^{(-)}$ to nS at lowest H, exponential solution to nS, the same exponential solution to another nS and K_3 to that nS – so all the regimes are singular in that case. Next case to consider is $\zeta = 1$, $\dot{H}(H)$ and $\dot{h}(H)$ for it are

presented on (f) and (g) panels. As we mentioned, in this case we have nonstandard singularity at H=0 so the regimes for h_+ branch, presented on (f) panel, are exponential to nS, exponential to another nS and K_3 to nS - same as above, we have no regimes with nonsingular future asymptote. On (g) panel we presented the behavior for h_- ; one can see that it is quite similar to Fig. 5(g) with the difference that at H=0 we now have nonstandard singularity instead of continuation to H<0. Finally, on (h) and (i) panels we present $\zeta>1$ regimes. As we mentioned while describing the denominator of \dot{H} and \dot{h} , now h_- branch could have zero in denominator and so nonstandard singularity appears on (i) panel. In some sense, one of two nonstandard singularities (see e.g. Fig. 6(e)) "moved" from h_+ branch to h_- and now both h_+ ((h) panel) and h_- ((i) panel) branches have nS. So for h_+ branch the regimes are expanding exponential to contracting exponential (derived with the same argumentation as $nS^{(-)}$ in previous cases), exponential to nS and K_3 to nS. For h_- branch, the regimes are nS to $nS^{(-)}$, nS to isotropic exponential solution and K_3 to this solution. This finalize our study of $\alpha>0$ regimes, on the remaining Fig. 7 we collected $\alpha<0$ cases.

So the first of $\alpha < 0$ cases to consider is the case $\zeta > 0$ presented in Fig. 7(a, b). We can see that, according to the h(H) description, its domain of definition does not reach H=0 and the regimes resemble those of $\alpha > 0$ case (compare with Fig. 5(a, b)). So the regimes for h_+ branch, presented on (a) panel, are nS to isotropic exponential solution and K_3 to the same exponential solution. Another branch, h_{-} , presented on (b) panel, demonstrates only K_3 to nS transition. The next distinct behavior corresponds to $0 > \zeta > -5/6$ and it presented in (c) and (d) panels $-h_{+}$ on (c) and h_{-} on (d). We can see that the domain of definition covers entire H>0. For h_{+} the regimes are $nS^{(-)}$ to nS (with the same reasoning as in previous cases), nS to isotropic exponential and K_3 to the same regime while for h_- they are isotropic exponential contraction to isotropic exponential expansion (similar to presented in Fig. 5(g)), and K_3 to the isotropic exponential expansion. Finally, last four panels correspond to $\zeta < -5/6$ case. From (e) and (f) panels we can see that it is the case with two-fold discontinuous domain of definition – we have one domain at lower H and another at higher. Panel (e) corresponds to h_+ while (f) – to h_- . Also, panel (g) shows fine structure of the feature on the higher-H branch from panel (e) while panel (h) - similar feature but from lower-H branch from panel (f). With all these taken into account, the list of regimes for h_+ branch includes $nS^{(-)}$ to nS at low H, nS to exponential solution, and K_3 to the same exponential solution. The regimes for h_{-} include exponential contraction to expansion – opposite to what we see in Fig. 6(h), nS to the same exponential solution and K_3 to another nS.

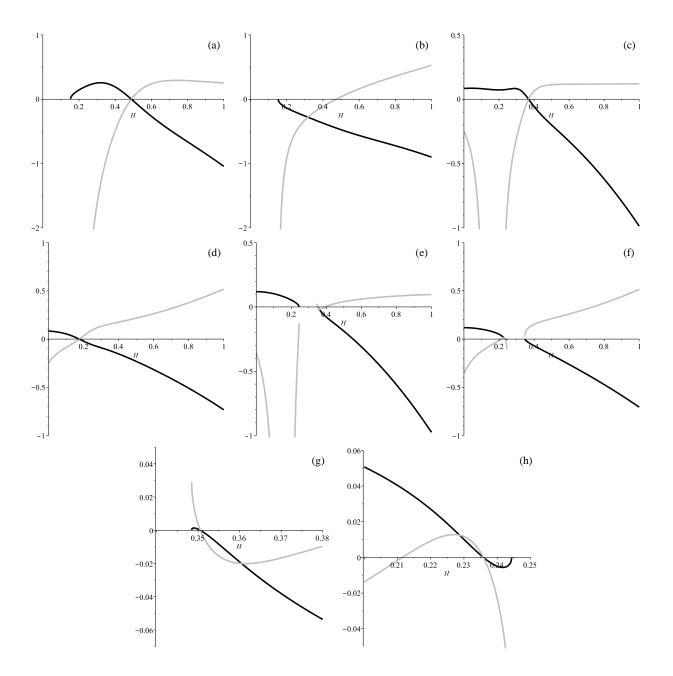


FIG. 7: Continuation of Figs. 5 and 6 for $\alpha < 0$ and: $\zeta > 0$ on (a) and (b) panels; $0 > \zeta > -5/6$ on (c) and (d) panels; $\zeta < -5/6$ on (e)–(h) panels (see the text for more details).

At this point it worth mentioning that all exponential solutions in this case are anisotropic, but if we take h(H) expressions and figures into account (Fig. 4), we can note that both H > 0 and h > 0 and in some cases we could even have h > H, so that it is unlikely for these solutions to give us proper dynamical compactification.

The situation changes at $\zeta \leqslant -3/2$ – at this point the exponential solution from h_- branch

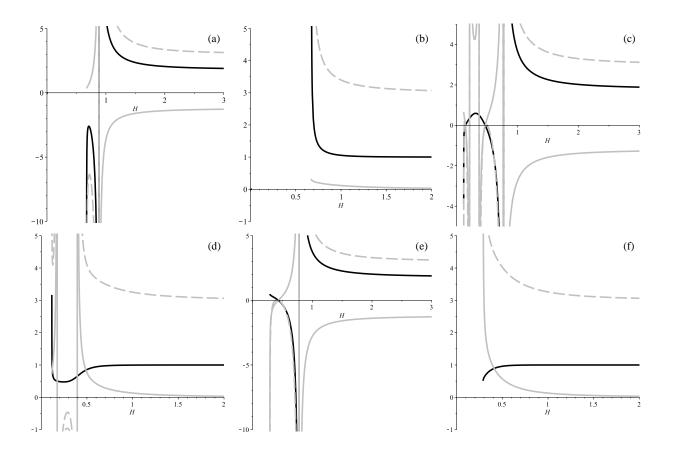


FIG. 8: Behavior of Kasner exponents in D=2 model for $\alpha>0$ and: $\zeta<\zeta_0$ on (a) and (b) panels; $0>\zeta>\zeta_0,\ \zeta\neq-1/6$ on (c) and (d) panels; $\zeta=-1/6$ on (e) and (f) panels (see the text for more details).

disappears, leaving h_- branch with just nonstandard singularities as future asymptotes. As of h_+ branch, at $\zeta = -3/2$ we have h = 0 and for $\zeta < -3/2$ we have h > 0 so the corresponding transition from the high-energy Kasner to the exponential solution becomes viable.

Finally, to complete description of this case we need to consider the dynamics in Kasner exponents. Being defined as $p = -H^2/\dot{H}$, they could be expressed through h(H) (see Eq.(19)), \dot{H} and \dot{h} (see Eqs. (21)–(22)) with p_H being Kasner exponent associated with H and p_h – with h. The analysis of \dot{H} and \dot{h} roots and asymptotes is applicable to p_H and p_h as well, so we present the resulting behavior of p_H and p_h in Figs. 8–11.

The analysis of these curves is quite similar to how we did it in D=1 case, so let us skip minor details. In Fig. 8 we presented cases for $\alpha>0$ and $\zeta<\zeta_0$ on (a) and (b) panels; $0>\zeta>\zeta_0$, $\zeta\neq-1/6$ on (c) and (d) panels; $\zeta=-1/6$ on (e) and (f) panels. We can see divergences of p_H and p_h at the locations of exponential solutions and $p_H=0$ with $p_h=0$ at nonstandard singularities. We also confirm K_3 regime at large H in all cases presented in Fig. 8.

The cases presented in Fig. 9 and further are more interesting. Indeed, starting from $\zeta > 0$ the domain of definition for \dot{H} and \dot{h} cover entire H > 0 in $\alpha > 0$ case, so that now we have $H \to 0$ solution. Taking appropriate limits, we can find limits for both $H \to 0$ and $H \to \infty$; we present them in Table II.

in sammer, or b = ir term pewer iam					
p_i	$H \rightarrow 0$	$H o \infty$			
	both branches	h_{+}	h_{-}		
p_H	0	$-\frac{9\alpha}{2\sqrt{\alpha^2-7\alpha}}$	$\frac{9\alpha}{2\sqrt{\alpha^2+7\alpha}}$		
p_h	$-\frac{2}{3}\alpha\Lambda + \frac{2}{3}$	$-\frac{3\sqrt{\alpha^2}+3\alpha}{5\alpha}$	$\frac{3\sqrt{\alpha^2} - 3\alpha}{5\alpha}$		
$\sum p$	$-\frac{4}{3}\alpha\Lambda + \frac{4}{3}$	3	3		

TABLE II: Summary of D=2 Λ -term power-law regimes.

One can clearly see that both high-energy regimes are Gauss-Bonnet Kasner with $\sum p = 3$. But low-energy regimes are not Kasner, as they do not have $\sum p = 1$. With $p_H = 0$ one can immediately confirm that $\sum p_i p_j p_k = 0$ for this case which makes it "generalized Milne" (see e.g. [20]). Recently it was demonstrated that in vacuum case this regime is forbidden [48], and our analysis of the vacuum case [55] confirms this. Let us also note that in all previous numerical studies [44, 45, 47, 49] we never detected this regime so this is the first time we see it. But also, this regime is not asymptotic (similar to the Kasner-like regimes in D = 1), so it is not really reached and the final asymptotic regime is either exponential with H < 0 or nonstandard singularity with H < 0, depending on the case.

Apart from these regimes, which could be clearly seen from, say, Figs. 9(c, d), we can observe usual components like divergences of p_H and p_h at the locations of the exponential solutions as well as zeros of p_H and p_h at the locations of nonstandard singularities. Figures 9(f, g) illustrate the situation with multiple exponential solutions. We skip the detailed description of all cases but confirm that the regimes correspond to the description in $\{\dot{H}, \dot{h}\}$.

In Fig. 11, which corresponds to $\alpha < 0$ case, we once again can see incomplete domain of definition: on (a) and (b) panels it is $H > H_0$ while on (e) and (f) panels it is $H \in [0; H_{0(1)}) \cup (H_{0(2)}; +\infty)$ – all according to the description in $\{\dot{H}, \dot{h}\}$.

Finally it is time to summarize all our regimes found. Due to enormous amount of different regimes we spread them into three tables – II, III and IV. In all tables we assume following notations: $H(\xi_i)$ is the value for Hubble parameter H derived from given value for ξ_i and for given value of α from $\xi_i = \alpha H^2$ relation. Individual ξ_i are described above and here we just recollect them: ξ_{\pm}

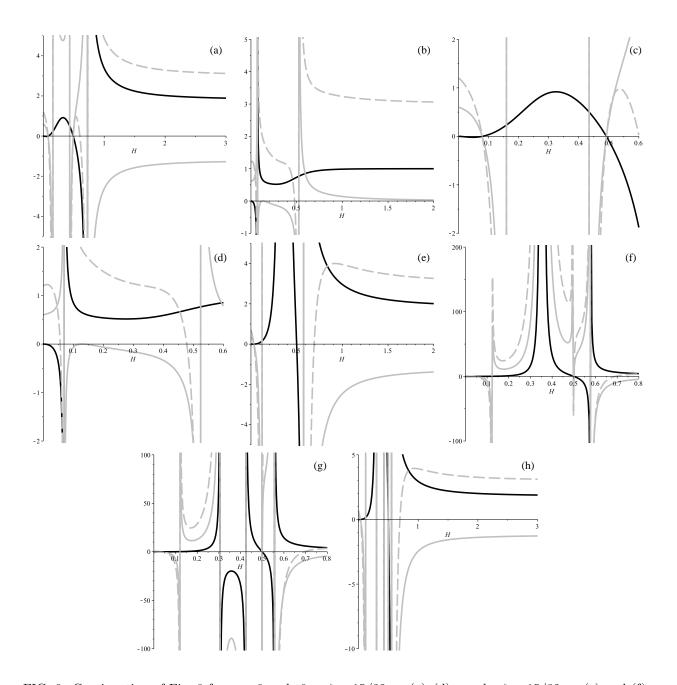


FIG. 9: Continuation of Fig. 8 for $\alpha > 0$ and: $0 < \zeta < 15/32$ on (a)–(d) panels; $\zeta = 15/32$ on (e) and (f) panels; $1/2 > \zeta > 15/32$ on (g) and (h) panels (see the text for more details).

are roots of the quadratic equation from (25), $\xi_{1,2,3}$ are roots of the cubic equation from (25), $\xi_{4,5}$ are roots of the denominator Q_{\pm} from (22). Positivity of the discriminant (20) is guaranteed by $H > H_0$ in case when there is only one positive root (like grey curve in Fig. 4(a)) and by $H < H_{0(1)}$ combined with $H > H_{0(2)}$ for the case when there are two roots (like black curve in Fig. 4(b)). Below we briefly comment on some regimes for each particular table.

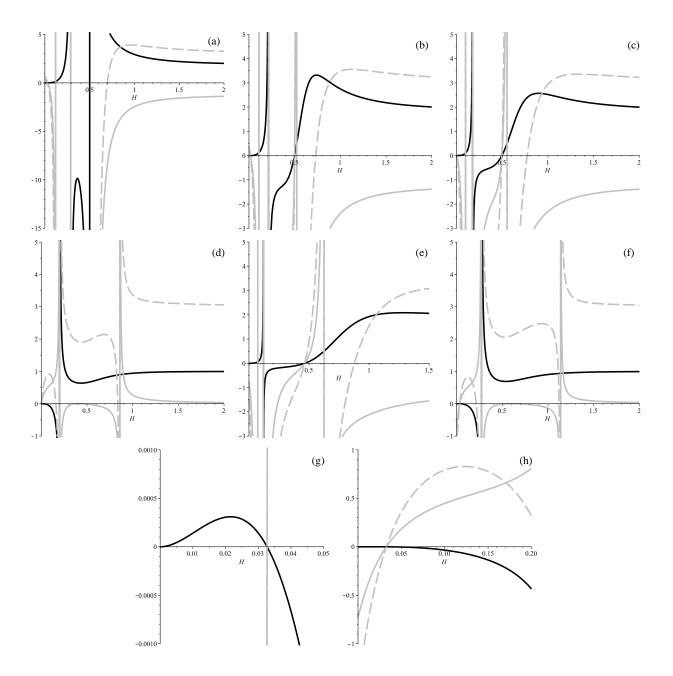


FIG. 10: Continuation of Figs. 8 and 9 for $\alpha > 0$ and: $\zeta = 1/2$ on (a) panel; $1 > \zeta > 1/2$ on (b) panel; $\zeta = 1$ on (c) and (d) panels; $\zeta > 1$ on (e)–(h) panels (see the text for more details).

In Table III we summarized $(\alpha > 0, \Lambda < 0)$ regimes. One can see that the only exponential solutions in that case are isotropic ones so they do not correspond to any physical cases.

In Table IV we summarized ($\alpha > 0$, $\Lambda > 0$) regimes. As we can see from Figs. 5 and 6, this case is most abundant with different regimes. We can detect up to three anisotropic exponential solutions for a single h_+ branch, plus isotropic solution on h_- branch for the same values of α and

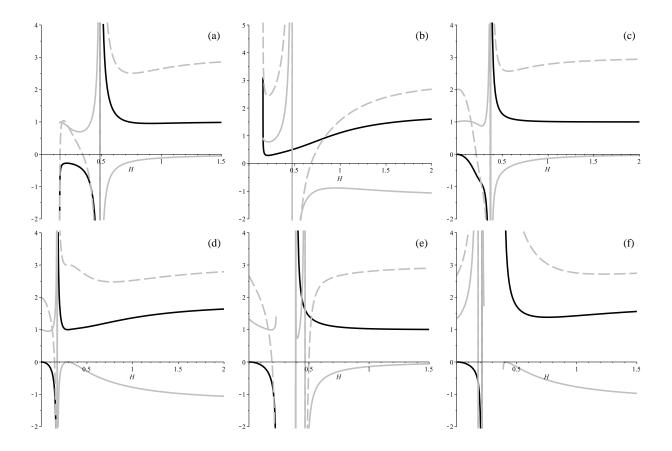


FIG. 11: Continuation of Figs. 8–10 for $\alpha < 0$ and: $\zeta > 0$ on (a) and (b) panels; $\zeta > -5/6$ on (c) and (d) panels; $\zeta < -5/6$ on (e) and (f) panels $\zeta > 1$ on (e)–(h) panels (see the text for more details).

 Λ . Also in this case we have $K_3 \to E$ transition – smooth transition from Gauss-Bonnet Kasner to anisotropic exponential solution – the only physically viable regime we detected. Let us also note that this regime exist only for $\alpha\Lambda \leq 1/2$.

Finally in Table V we presented the results for $\alpha < 0$. In there, E_2 and E_3 exponential solutions require additional clarification – they are anisotropic but they give $h_{\pm}/H > 0$, so that both three-dimensional and extra-dimensional manifolds are expanding. We treat it as violation of viability and so discard them. This situation is partially change for $\alpha \Lambda \leq -3/2$ – in that case E_3 solution (on h_+ branch) change its sign to $h_+/H \leq 0$ while its E_2 counterpart disappears. Also, for exact $\alpha \Lambda = -3/2$ relation we have $h(t) \to 0$, in which we recover the regime quite similar to "geometric frustration" one, described in [26]. We discuss it further is Discussions section.

This finalize our study of D=2 Λ -term regimes. Unlike D=1 case, now we have physically viable regimes $K_3 \to E$. Generally, the dynamics is much more abundant then in both D=1 case and D=2 vacuum counterpart [55]. We discuss this, as well as D=1 cases, in detail below.

Branch Additional conditions Regimes $H < H_0$ no solutions $\alpha \Lambda \lessapprox -0.17$ $H(\xi_-) > H > H_0$ $nS \to E_{iso}$ $H > H(\xi_-)$ $K_3 \to E_{iso}$ $H < H_0$ no solutions $nS \to nS$ $H(\xi_4) > H > H_0$ $H(\xi_5) > H > H(\xi_4)$ $nS \to nS$ $H(\xi_-) > H > H(\xi_5)$ $nS \to E_{iso}$ $H > H(\xi_-)$ $K_3 \rightarrow E_{iso}$ $H < H_0$ no solutions $H(\xi_{4,5}) > H > H_0$ $nS \to nS$ $\alpha\Lambda = -1/6$ $H(\xi_{-}) > H > H(\xi_{4,5})$ $nS \to E_{iso}$ $H > H(\xi_-)$ $K_3 \to E_{iso}$ $H < H_0$ no solutions h_{-} $H > H_0$ $K_3 \to nS$

TABLE III: Summary of D = 2 ($\alpha > 0$, $\Lambda < 0$) Λ -term regimes.

V. DISCUSSIONS

In this paper we have considered Einstein-Gauss-Bonnet cosmological model with D=1 and D=2 extra dimensions in presence of Λ -term. In this section we summarize our finding and discuss them. Before discussing each particular case, let us make several important notes. First one is related to the power-law solutions. We can clearly see that in both cases, unlike vacuum regimes [55], we do not have low-energy Kasner regimes. But this is natural – indeed, in presence of Λ -term it will eventually start to dominate and turn any low-energy regime into the exponential one. Also, formal consideration of power-law regimes in pure Gauss-Bonnet gravity (see, e.g., [20, 47, 48]) forbid power-law regimes to exist in presence of Λ -term. Indeed, if we consider, say, constraint equation $\sum H_i H_j H_k H_l = \rho$ in power-law $Ansatz \ a_i(t) \propto t^{p_i}$, it takes the form $t^{-4} \sum p_i p_j p_k p_l = \rho$. Now one can see that in vacuum $(\rho = 0)$ we can cancel t^{-4} and arrive just to $\sum p_i p_j p_k p_l = 0$ well-known condition for the power-law solutions to exist in vacuum Gauss-Bonnet gravity. If ρ is dynamical, say, perfect fluid, constraint equation also could be solved under additional relation between the equation of state and sum of Kasner exponents [47]. But if ρ is nonzero constant (Λ -term), constraint equation cannot be solved for constant p_i and Λ , which means power-law solutions

TABLE IV: Summary of $D=2~(\alpha>0,~\Lambda>0)$ Λ -term regimes.

Branch	Addition	Regimes	
		$H < H(\xi_4)$	$nS^{(-)} \to nS$
		$H(\xi_5) > H > H(\xi_4)$	$nS \rightarrow nS$
	$\alpha\Lambda < 15/32$	$H(\xi_1) > H > H(\xi_5)$	$nS \to E_1$
		$H > H(\xi_1)$	$K_3 \rightarrow E_1$
		$H < H(\xi_4)$	$nS^{(-)} \to nS$
	$\alpha\Lambda=15/32$	$H(\xi_{2,3}) > H > H(\xi_4)$	$E_{2,3} \rightarrow nS$
		$H(\xi_5) > H > H(\xi_{2,3})$	$nS \rightarrow E_{2,3}$
		$H(\xi_1) > H > H(\xi_5)$	$nS \to E_1$
		$H > H(\xi_1)$	$K_3 \to E_1$
		$H < H(\xi_4)$	$nS^{(-)} \to nS$
		$H(\xi_2) > H > H(\xi_4)$	$E_2 \to nS$
	$1/2 > \alpha \Lambda > 15/32$	$H(\xi_3) > H > H(\xi_2)$	$E_2 \to E_3$
		$H(\xi_5) > H > H(\xi_3)$	$nS \to E_3$
		$H(\xi_1) > H > H(\xi_5)$	$nS \to E_1$
h_{+}		$H > H(\xi_1)$	$K_3 \to E_1$
	$\alpha\Lambda=1/2$	$H < H(\xi_4)$	$nS^{(-)} \to nS$
		$H(\xi_{2,3}) > H > H(\xi_4)$	$E_{2,3} \to nS$
		$H(\xi_1) > H > H(\xi_{2,3})$	$E_1 \rightarrow E_{2,3}$
		$H > H(\xi_1)$	$K_3 \to E_1$
		$H < H(\xi_4)$	$nS^{(-)} \to nS$
	$1 > \alpha \Lambda > 1/2$	$H(\xi_{\{1,3\}}) > H > H(\xi_4)$	$E_{\{1,3\}} \to nS$
	$1 > \alpha \Lambda > 1/2$	$H(\xi_5) > H > H(\xi_{\{1,3\}})$	$E_{\{1,3\}} \to nS$
		$H > H(\xi_5)$	$K_3 \to nS$
		$H < H(\xi_1)$	$E_1 \to nS$
	$\alpha\Lambda = 1$	$H(\xi_5) > H > H(\xi_1)$	$E_1 \to nS$
		$H > H(\xi_5)$	$K_3 \to nS$
		$H < H(\xi_1)$	$E_1 \to E_1^{(-)}$
	$\alpha\Lambda > 1$	$H(\xi_5) > H > H(\xi_1)$	$E_1 \to nS$
		$H > H(\xi_5)$	$K_3 \rightarrow nS$
	$\alpha\Lambda < 1$	$H < H(\xi_+)$	$E_{iso}^{(-)} \to E_{iso}$
		$H > H(\xi_+)$	$K_3 \to E_{iso}$
h	$\alpha\Lambda = 1$	$H < H(\xi_+)$	$nS \to E_{iso}$
		$H > H(\xi_+)$	$K_3 \rightarrow E_{iso}$
		$H < H(\xi_4)$	$nS \to nS^{(-)}$
	$\alpha\Lambda > 1$	$H(\xi_1) > H > H(\xi_4)$	$nS \to E_{iso}$
		$H > H(\xi_1)$	$K_3 \to E_{iso}$

TABLE V: Summary of $D=2~\alpha<0~\Lambda$ -term regimes.

Λ	Branch	Additional	Regimes	
$\Lambda < 0$	h_+	$H \leftarrow$	no solutions	
		$H(\xi_{4,5})$:	$nS \rightarrow nS$	
		$H(\xi_{-}) >$	$nS \to E_{iso}$	
		H >	$K_3 \rightarrow E_{iso}$	
	h_{-}	H <	no solutions	
		H :	$K_3 \to nS$	
	h_{+}	$\alpha\Lambda\geqslant -5/6$	$H < H(\xi_4)$	$nS^{(-)} \to nS$
			$H(\xi_+) > H > H(\xi_4)$	$nS \to E_{iso}$
			$H > H(\xi_+)$	$K_3 \to E_{iso}$
		$\alpha \Lambda < -5/6$	$H < H_{\xi_{4,5}}$	$nS^{(-)} \to nS$
			$H_{0(1)} > H > H(\xi_{4,5})$	$nS \to nS$
			$H_{0(2)} > H > H_{0(1)}$	no solutions
			$H(\xi_3) > H > H_{0(2)}$	$nS \to E_3$
			$H > H(\xi_3)$	$K_3 \to E_3$
$\Lambda > 0$	h	$\alpha\Lambda\geqslant -5/6$	$H < H(\xi)$	$E_{iso}^{(-)} \to E_{iso}$
			$H > H(\xi)$	$K_3 \to E_{iso}$
		$-3/2 < \alpha \Lambda < -5/6$	$H < H(\xi_2)$	$E_2^{(-)} \to E_2$
			$H_{0(1)} > H > H(\xi_2)$	$nS \to E_2$
			$H_{0(2)} > H > H_{0(1)}$	no solutions
			$H > H_{0(2)}$	$K_3 \to nS$
		$\alpha\Lambda\leqslant -3/2$	$H < H_{0(1)}$	$nS^{(-)} \to nS$
			$H_{0(2)} > H > H_{0(1)}$	no solutions
			$H > H_{0(2)}$	$K_3 \to nS$

cannot exist in presence of Λ -term. Yet, we clearly see them – at least, K_3 . This could be explained as follows: Λ -term is constant while we have dynamical evolution for H. And in high-energy regime $H_i \gg \Lambda$ so that we could consider $\Lambda/H_i \approx 0$ in that case and recover Gauss-Bonnet power-law solutions.

Another surprise with power-law solutions is the existence of the generalized Milne-like solutions, although unstable. In [48] we clearly demonstrated that in vacuum, the generalized Milne solution cannot exist as it leads to degenerative system with unconstrained Hubble parameters. It was decided that this is an artifact caused by the fact that we neglect lower-order contribution while

building power-law solutions. Yet, we detected these solutions, although as an intermediate regime between nonstandard singularities or exponential solutions.

Other important notes regard exponential solutions. First, in D=2 case exponential solutions are governed by two equations – quadratic and cubic. On contrary, in our paper dedicated to the exponential solutions in lower-dimensional Einstein-Gauss-Bonnet cosmologies [50], exponential solutions for this case are reported to be governed by cubic equation alone (one can check that the cubic equations from this paper and from [50] are the same). In this paper anisotropic solutions are governed by the roots of this cubic while isotropic – only by roots of this quadratic, but potentially in other cases additional roots could give rise to additional exponential solutions, so additional study of exponential solutions in both Einstein-Gauss-Bonnet and more general Lovelock gravity is required.

Another note which regard exponential solutions is related to their stability. Indeed, stability of exponential solutions was addressed in [53] and the results for vacuum case [55] are in perfect agreement with them. Yet, from Figs. 5 and 6 one can clearly see directional stability or even instability of certain exponential solutions for $15/32 \ge \zeta \ge 1/2$. We have not reported any cases of the directional stability in [53], but see them in current research from phase portraits; this also require additional investigation.

As a final point, we want to stress readers' attention to the situation we call "nonstandard singularity". As we can see from the equations of motion (4), they are nonlinear with respect to the highest derivative³, so formally we can solve them with respect to the highest derivative. Then, the highest derivative is expressed as a ratio of two polynomials, both depending on H. And there could be a situation when the denominator of this expression is equal to zero while numerator is not. In this case \dot{H} diverges while H is (generally) nonzero and regular. In our study we saw nonstandard singularities with divergent \dot{h} or both \dot{h} and \dot{H} at nonzero or sometimes zeroth H. This kind of singularity is "weak" by Tipler's classification [59], and "type II" in classification by Kitaura and Wheeler [60, 61]. Recent studies of the singularities of this kind in the cosmological context in Lovelock and Einstein-Gauss-Bonnet gravity demonstrates [27, 44, 45, 47, 49] that their presence is not suppressed and they are abundant for a wide range of initial conditions and parameters and

³ Actually, this is one of the definitions of Lovelock (and Gauss-Bonnet as its particular case) gravity: it is well-known [56–58] that the Einstein tensor is, in any dimension, the only symmetric and conserved tensor depending only on the metric and its first and second derivatives (with a linear dependence on second derivatives). If one drops the condition of linear dependence on second derivatives, one can obtain the most general tensor which satisfies other mentioned conditions – Lovelock tensor [16].

sometimes [45] they are the only option for future behavior.

With these points noted, let us turn to summarizing particular cases. First of them, D=1case, have GB Kasner K_3 as the only high-energy regime and singular Kasner-like \tilde{K}_1^S regime as the only low-energy regime. This makes the difference between this and the vacuum cases – the latter have non-singular low-energy Kasner regime and so have smooth transition between high- and low-energy regimes. The Λ -term D=1 case lacks this transition so we cannot restore Friedmann-like behavior in this case. Intermediate-energy regimes include nonstandard singularities and exponential regimes, and the latter are presented only by isotropic regimes. This is expected - indeed, in [50] we demonstrated that for Λ -term D=1 model there are two possible exact exponential solutions – isotropic solution and anisotropic one, but the latter with $h \in \mathbb{R}$. The fact that h is unconstrained feels unphysical and later in [53] it was demonstrated that anisotropic solution is marginally/neutrally stable. Finally in this study we clearly demonstrate that this solution formally exist but is never reached. So that it is natural to extend this conclusion on other exponential solutions from [50, 52] with one or more unconstrained Hubble parameters – they are unphysical and cannot be reached which leaves us only with solutions proven to be stable in [53]. What was unexpected is the presence of two distinct isotropic exponential solutions in D=1 case - it cannot be seen from the study of exact exponential solutions [50], but here we detect them. This fact also indicate that additional study of exponential solutions is required. So that in D=1case we have no viable late-time regimes – the only nonsingular regime is isotropic exponential expansion and it is definitely not what we observe.

Another case considered is D=2. It is very different from D=1 both in power-law and exponential solutions. The former of them have GB Kasner K_3 , just like D=1, but similarities end here. Unlike D=1 case, D=2 one does not have stable low-energy regime. Indeed, we saw that H=0 point in D=2 is regular point of dynamical evolution and so the dynamics is prolonged to H<0 domain. This is very different from what we saw in vacuum [55] and D=1 Λ -term cases. Indeed, checking h(H) and H(h) expressions and curves in vacuum case [55] clearly demonstrate that there are only two options – either $H\to 0$ with $h\to 0$, which gives us regular low-energy Kasner regime K_1 , or $H\to 0$ with $h\to \pm \infty$, which gives us singular low-energy Kasner regime⁴. On contrary, from (19) and Figs. 4(e)–(i) one can see that in D=2 case for $H\to 0$ we have regular and nonzero h. This results in absence of regular low-energy (power-law) regime and

⁴ Singular low-energy Kasner regime arises from negative Kasner exponent p_i – indeed, in case $p_i < 0$ we have $a_i(t) \propto 1/t^{\alpha_i}$ with $\alpha_i = -p_i > 0$, making $a_i(t)$ divergent at t = 0.

in another feature, which we discuss a bit later.

So that the regimes which reach H = 0 continue to H < 0 domain and, due to the $H \to -H$ symmetry of the equations of motion (21)–(24), face the regime which is dual to the closest to H = 0. Since the only regimes that could be presented are nonstandard singularity or exponential solution, possible transitions include pairwise evolution between such singularities and expanding/contracting exponential solutions. In reality we have contracting isotropic exponential solution anisotropically bounce to expanding isotropic exponential solution (see Fig. 5(g) and Fig. 7(d)) as well as anisotropic solution with expanding three-dimensional space transits to regime with contracting three-dimensional space (see Fig. 6(h) and the opposite – contracting transits to expanding (see Fig. 7(f, h).

For the regimes which do not reach H=0, future evolution is represented by either nonstandard singularities or exponential solutions. The former of them cannot correspond to a viable regime but some of the latter can. In D=1 case we have only isotropic solutions but D=2 abundant with anisotropic ones as well. For $\alpha > 0$, $\Lambda < 0$ there are only isotropic solutions (see Table III) but in $\alpha > 0$, $\Lambda > 0$ case there are up to three different anisotropic solutions. This number comes from the number of possible roots of bicubic equation and is in agreement with [50]. Let us note that in this case anisotropic solutions exist only for $\alpha\Lambda \leq 1/2$ and only in h_+ branch (see Table IV); h_{-} branch has isotropic solutions only. Finally for $\alpha < 0$, as we can see from Table V, for $\Lambda < 0$ we have only isotropic solutions for h_+ and no exponential solutions for h_- . For $\Lambda > 0$ situation changes a bit: for both branches we have isotropic solution for $\alpha \Lambda \geqslant -5/6$ and anisotropic for $\alpha \Lambda < -5/6$. One of these two anisotropic solutions (E_2 on h_- branch) always have h(t) > 0 while another $(E_3 \text{ on } h_+ \text{ branch})$ – only as long as $\alpha \Lambda > -3/2$, because at $\alpha \Lambda < -3/2$ it has h(t) < 0and so contraction of extra dimensions is restored. Also, from Table V one can see that only E_3 is the "endpoint" for $K_3 \to E_3$ transition while E_2 does not have high-energy regime as a past asymptote. At $\alpha\Lambda = -3/2$, E_2 solution disappears while E_3 solution has $h(t) \to 0$ so that extra dimensions "stabilize" – their "size" (in terms of the scale factor) reaches some constant value. This is very similar to the stabilization of the extra dimensions size due to the "geometric frustration", described in [26] and further analyzed in [27, 28]. But these two cases have a huge difference – "geometric frustration" case have negative spatial curvature of extra dimensions and special range of couplings while this case is spatially flat and we have exact relation between the couplings. The regime with constant-size extra dimensions is of additional importance – in case if extra dimensions are topologically compact, the total action could be expressed as four-dimensional action plus some corrections – the similar way as it is done for Kaluza-Klein theory. If it is done, one could pose additional constraints on the theory from accelerator physics.

Let us note that we have not seen solutions of this type (with $h(t) \to 0$) neither in vacuum case [55] nor in D=1 case – it is another feature of h(H) relation in D=2 case, discussed above. Indeed, if we substitute h=0 into the general constraint equation (8), it takes the form $6H^2=\Lambda$ – so that in vacuum case it is always H=0 – either K_1 or nonstandard singularity. If we further substitute h=0 and $6H^2=\Lambda$ into one of the dynamical equations (6), it takes the form $\dot{H}=0$ – in both vacuum and Λ -term cases. In the former of them we additionally have H=0 which corresponds to the low-energy Kasner regime while in the latter we have $H\neq 0$ which corresponds to the exponential solution. But this scheme does not worked for D=1 Λ -term case due to degeneracy between H and h – it is lowest-dimensional case and in higher dimensions $D\geqslant 2$ this degeneracy is removed.

VI. CONCLUSIONS

To conclude, we performed thorough analysis of Λ -term regimes in Einstein-Gauss-Bonnet gravity in two lowest number of dimensions – five and six. We have considered the manifold which is a product of three-dimensional (which represents our Universe) and extra-dimensional (in our case with D=1, 2 dimensions) parts. This separation is quite natural as with it we could describe natural compactification. Our analysis demonstrate that generally Λ -term models have much mode abundant dynamics then vacuum cases [55]. Our investigation also suggest that in D=1 model there are no physically viable regimes. On contrary, D=2 case have smooth transitions from high-energy Kasner regime to anisotropic exponential solutions with contracting extra dimensions. In one particular case $\alpha\Lambda = -3/2$ with $\alpha < 0$ and $\Lambda > 0$ the size of extra dimensions (in the sense of the scale factor) reaches constant value (and so the expansion rate $h(t) \to 0$), making this case similar to the regime described in spatially-curved "geometric frustration" model [26].

Both D=1 and D=2 cases lack regular low-energy regime – in the former of them it is singular (one faces finite-time singularity while reaching low-energy Kasner regime) and for the latter H=0 is not an endpoint and the evolution continues to H<0 domain until either nonstandard singularity or exponential solution is reached. So that in D=2 case we have interesting regimes like the transition from isotropic exponential contracting to isotropic exponential expansion (like a bounce) and anisotropic regimes with contracting three-dimensional spaces turn to expansion and vice versa.

Lack of low-energy regimes in D=2 as well as presence of h=0 anisotropic exponential solution have the same cause -h(H) expression in D=2 case is distinct from both D=1 and the entire vacuum case [55]. Indeed, in both D=1 and the vacuum case, h(H) and H(t) curves have either $h\to 0$ or $h\to \pm\infty$ as $H\to 0$. In the former case we have low-energy nonsingular Kasner regime, in the latter – the same but singular. Also one can see that we cannot have h=0 while $H\neq 0$, which prevent corresponding exponential solutions to exist. On contrary, one can see that in D=2 we have $h\neq 0$ at H=0 so that h=0, $H\neq 0$ exponential solutions exist while low-energy regimes are absent. With the same argumentation, h=0, $H\neq 0$ exponential solutions could exist in higher-order Lovelock models as well, except for lowest possible dimensions, like D=3 for cubic Lovelock, D=4 for quadric and so on.

Overall, present study brought us several unexpected results – for power-law solutions, we found singular low-energy Kasner-like behavior for D=1 and Milne-like behavior for D=2. Both regimes are supposed to be forbidden to exist in presence of Lambda-term, yet the analysis in term of Kasner exponents points on them. Of course, none of these regimes are reached, but the fact that analysis points on them could indicate that they formally could exist but are unstable – so this situation is in need for the additional investigation. Exponential solutions also behave not exactly as expected – multiple distinct isotropic solutions for both D=1 and D=2 as well as directional stability of anisotropic solutions in D=2 clearly indicate need of additional study of exponential solutions as well.

Low-dimensional Λ -term case demonstrated interesting dynamics for both D=1 and D=2 with some unexpected features. In forthcoming paper we consider D=3 and generic $D\geqslant 4$ Λ -term cases and finalize our study Λ -term case.

Acknowledgments

This work was supported by FAPEMA under project BPV-00038/16.

^[1] G. Nordström, Phys. Z. 15, 504 (1914).

^[2] G. Nordström, Ann. Phys. (Berlin) **347**, 533 (1913).

^[3] A. Einstein, Ann. Phys. (Berlin) **354**, 769 (1916).

^[4] T. Kaluza, Sit. Preuss. Akad. Wiss. **K1**, 966 (1921).

^[5] O. Klein, Z. Phys. **37**, 895 (1926).

- [6] O. Klein, Nature (London) 118, 516 (1926).
- [7] J. Scherk and J.H. Schwarz, Nucl. Phys. **B81**, 118 (1974).
- [8] M.A. Virasoro, Phys. Rev. 177, 2309 (1969).
- [9] J.A. Shapiro, Phys. Lett. **33B**, 361 (1970).
- [10] P. Candelas, G.T. Horowitz, A. Strominger and E. Witten, Nucl. Phys. B258, 46 (1985).
- [11] D.J. Gross, J.A. Harvey, E. Martinec and R. Rohm, Phys. Rev. Lett. 54, 502 (1985).
- [12] B. Zwiebach, Phys. Lett. **156B**, 315 (1985).
- [13] C. Lanczos, Z. Phys. **73**, 147 (1932).
- [14] C. Lanczos, Ann. Math. 39, 842 (1938).
- [15] B. Zumino, Phys. Rep. **137**, 109 (1986).
- [16] D. Lovelock, J. Math. Phys. (N.Y.) **12**, 498 (1971).
- [17] F. Müller-Hoissen, Phys. Lett. **163B**, 106 (1985).
- [18] N. Deruelle and L. Fariña-Busto, Phys. Rev. D 41, 3696 (1990).
- [19] F. Müller-Hoissen, Class. Quant. Grav. 3, 665 (1986).
- [20] S.A. Pavluchenko, Phys. Rev. D 80, 107501 (2009).
- [21] J. Demaret, H. Caprasse, A. Moussiaux, P. Tombal, and D. Papadopoulos, Phys. Rev. D 41, 1163 (1990).
- [22] G. A. Mena Marugán, Phys. Rev. D 46, 4340 (1992).
- [23] E. Elizalde, A.N. Makarenko, V.V. Obukhov, K.E. Osetrin, and A.E. Filippov, Phys. Lett. B644, 1 (2007).
- [24] K.I. Maeda and N. Ohta, Phys. Rev. D 71, 063520 (2005).
- [25] K.I. Maeda and N. Ohta, JHEP **1406**, 095 (2014).
- [26] F. Canfora, A. Giacomini and S. A. Pavluchenko, Phys. Rev. D 88, 064044 (2013).
- [27] F. Canfora, A. Giacomini and S. A. Pavluchenko, Gen. Rel. Grav. 46 1805 (2014).
- [28] F. Canfora, A. Giacomini, S. A. Pavluchenko and A. Toporensky, arXiv:1605.00041.
- [29] D.G. Boulware and S. Deser, Phys. Rev. Lett. **55**, 2656 (1985).
- [30] J.T. Wheeler, Nucl. Phys. **B268**, 737 (1986).
- [31] R.G. Cai, Phys. Rev. D 65, 084014 (2002).
- [32] T. Torii and H. Maeda, Phys. Rev. D 71, 124002 (2005).
- [33] T. Torii and H. Maeda, Phys. Rev. D 72, 064007 (2005).
- [34] D.L. Wilshire. Phys. Lett. **B169**, 36 (1986).
- [35] R.G. Cai, Phys. Lett. **582**, 237 (2004).
- [36] J. Grain, A. Barrau, and P. Kanti, Phys. Rev. D 72, 104016 (2005).
- [37] R.G. Cai and N. Ohta, Phys. Rev. D 74, 064001 (2006).
- [38] H. Maeda, Phys. Rev. D **73**, 104004 (2006).
- [39] M. Nozawa and H. Maeda, Class. Quant. Grav. 23, 1779 (2006).

- [40] H. Maeda, Class. Quant. Grav. 23, 2155 (2006).
- [41] M.H. Dehghani and N. Farhangkhah, Phys. Rev. D 78, 064015 (2008).
- [42] H. Ishihara, Phys. Lett. **B179**, 217 (1986).
- [43] N. Deruelle, Nucl. Phys. **B327**, 253 (1989).
- [44] S.A. Pavluchenko and A.V. Toporensky, Mod. Phys. Lett. A24, 513 (2009).
- [45] S.A. Pavluchenko, Phys. Rev. D 82, 104021 (2010).
- [46] V. Ivashchuk, Int. J. Geom. Meth. Mod. Phys. 07, 797 (2010) arXiv: 0910.3426.
- [47] I.V. Kirnos, A.N. Makarenko, S.A. Pavluchenko, and A.V. Toporensky, General Relativity and Gravitation 42, 2633 (2010).
- [48] S.A. Pavluchenko and A.V. Toporensky, Gravitation and Cosmology 20, 127 (2014); arXiv: 1212.1386.
- [49] I.V. Kirnos, S.A. Pavluchenko, and A.V. Toporensky, Gravitation and Cosmology 16, 274 (2010) arXiv: 1002.4488.
- [50] D. Chirkov, S. Pavluchenko, A. Toporensky, Mod. Phys. Lett. A29, 1450093 (2014); arXiv: 1401.2962.
- [51] D. Chirkov, S. Pavluchenko, A. Toporensky, Gen. Rel. Grav. 46 1799 (2014); arXiv: 1403.4625.
- [52] D. Chirkov, S. Pavluchenko, A. Toporensky, Gen. Rel. Grav. 47 137 (2015); arXiv:1501.04360.
- [53] S.A. Pavluchenko, Phys. Rev. D **92**, 104017 (2015).
- [54] V. D. Ivashchuk, arXiv:1607.01244.
- [55] S.A. Pavluchenko, Phys. Rev. D **94**, 024046 (2016); arXiv:1605.01456
- [56] H. Vermeil, Nachr. Ges. Wiss. Göttingen (Math.-Phys. Klasse, 1917), p. 334.
- [57] H. Weyl, Raum, Zeit, Materie, 4th ed. (Springer, Berlin, 1921).
- [58] E. Cartan, J. Math. Pure Appl. 1, 141 (1922).
- [59] F.J. Tipler, Phys. Lett. **A64**, 8 (1977).
- [60] T. Kitaura and J.T. Wheeler, Nucl. Phys. **B355**, 250 (1991).
- [61] T. Kitaura and J.T. Wheeler, Phys. Rev. D 48, 667 (1993).